Int. J. Adv. Appl. Math. and Mech. 11(1) (2023) 1 – 21 (ISSN: 2347-2529)

Journal homepage: www.ijaamm.com

International Journal of Advances in Applied Mathematics and Mechanics

Electrohydrodynamic Instability of Rivlin-Ericksen Viscoelastic Dielectric Liquid Sheet in Relative Motion to Surrounding Inviscid Dielectric Gas Medium

Research Article

Mohamed F. El - Sayed[a, b, *], **Doaa M. Mostafa**[a, b], **Asma S. Al-Fowzan**[a]

[a] *Department of Mathematics, College of Science, Qassim University, P. O. Box 6644, Buraidah 51452, Saudi Arabia*

[b] *Department of Mathematics, Faculty of Education, Ain Shams University, P. O. Box 11341, Heliopolis (Roxy), Cairo, Egypt*

Received 20 March 2023; accepted (in revised version) 09 April 2023

Abstract: The purpose of this work is to theoretically and quantitatively investigate the linear electrohydrodynamic instability of a viscoelastic dielectric liquid sheet of the Rivlin-Ericksen type flowing with relative velocity to the surrounding inviscid dielectric gas medium. The method of normal modes analysis has been used to generate the differential equations characterizing the liquid and gas media and the electric field. This has been done in addition to Maxwell's equations and the appropriate boundary conditions at the fluid interfaces. These differential equations' solutions have been found, and dispersion relations between wave numbers and growth rates have been constructed for both situations and symmetric and antisymmetric disturbances. As a result of their extreme complexity, the resulting dispersion relations cannot be used to examine the stability of the system under consideration in an analytical manner. The dispersion relations are then first written in non-dimensional forms, and they are then numerically solved using a new method utilizing the Mathematica program. In-depth research has been done on how all of the analysis's factors affect the growth rates of disturbances in both two- and three-dimensional scenarios. It is discovered that the electric field, the Weber numbers, and the ratio of gas to liquid density all have destabilizing effects for both symmetric and antisymmetric modes of disturbance. The Ohnesorge number and the gas to liquid velocity ratio are shown to have a dual function in the stability of the system, whilst the viscoelasticity parameter is found to have stabilizing effects for both forms of disturbances.

MSC: 76A10 • 76E25 • 76W05 • 76S05

Keywords: Electrohydrodynamics • Liquid sheet instability • Viscoelastic fluids • Dielectric fluids

1. Introduction

A sheet of liquid can form when a dense fluid is ejected into a less dense fluid through a small slit whose thickness is significantly smaller than its width. In biological applications and astrophysical phenomena, the linear scale of a sheet can range from light years to nanometers [1]. The associated fluids can be anything from a complicated charged plasma subject to intense electromagnetic and gravitational forces to a tiny collection of basic molecules moving around freely with minimal external influence. Because of its intrinsic instability, the fluid sheet easily breaks apart. Knowing the physical mechanism of breakup is therefore quite helpful when one needs to fully utilize the phenomena, aside from its basic scientific significance [2]. Film coating, nuclear safety curtain production, spray combustion,

* Corresponding author.
E-mail address(es): mfahmye@hotmail.com (Mohamed F. El - Sayed).

agricultural sprays, ink jet printing, fiber and sheet drawing, processing powdered milk, powder metallurgy, toxic substance removal, and encapsulation of biomedical materials are a few examples of recent applications [3]. Books on the subject typically concentrate on particular applications because there are so many different uses. For instance, Lefebvre's [4] book discusses internal combustion, Masters' [5] book concentrates on the formation of powdered milk, Yarin's [6] book offers a mathematical analysis of recent applications involving non-Newtonian fluids, and Lin's [7] review book discusses the breakdown of both liquid sheets and jets. See the investigations by Li and Tankin [8], Cousin and Dumouchel [9], and more recently by Dasgupta et al. [10] and Han [11] for early research on the liquid sheets instability of viscous fluids.

A branch of fluid mechanics called electrohydrodynamic examines how electric and hydrodynamic forces interact. Due to its application in the sciences, it is a crucial branch. Electric phenomena and hydrodynamic motion are thus connected. As a result, there are two categories for electrohydrodynamic equations of motion. The first set consists of equations related to hydrodynamics and second-order responses to electric fields. The accompanying boundary conditions reflect how the sets of equations are coupled. Melcher [12], El-Sayed [13], and Moatimid et al. [14] each provide an overview of electrohydrodynamics with specific references to many of the recent advancements in the subject. In the meantime, the field of spray engineering has called for a thorough electrohydrodynamical examination into the mechanism behind the phenomena of liquid sheet disintegration in gas flow [15–19]. The electro-fluid dynamics of biological systems, the ejection of liquid in zero gravity environments, and insulation studies in liquids and gases are just a few examples of the many disciplines where electrohydrodynamics is applied. Due to these facts, there is an increasing demand for original research on the fundamental electrohydrodynamic phenomena involving the use of non-Newtonian fluids, which are the foundation for applications in the agricultural industry, biomedicine, etc. Since the interaction between the fluid and elasticity in the presence of an electric field is so complex, little is understood about the instability and breakdown of electrohydrodynamic non-Newtenian liquid sheets [20–25].

There are numerous viscoelastic fluids that neither Oldroyd's constitutive relations nor Maxwell's constitutive relations can adequately describe. Rivlin-Ericksen fluid is one of these viscoelastic fluids [26]; given its growing use in the production of spacecraft components (such as cushions, ropes, tyres, foams, seats, engineering equipment, airplanes, belt conveyers, contact lenses, etc.), it is desirable to investigate this fluid's instability. For engineers and applied mathematicians who are interested in finding precise solutions, studying the flow problems of this kind of viscoelastic fluid is not only crucial from a technological standpoint [27], but it is also difficult. Despite a few research on the instability analysis of viscoelastic liquid sheets, relevant literature reveals that the impacts of gas velocities and electric fields have largely been disregarded [28, 29].

Therefore, the current study's objective is to conduct an investigation of linear temporal electrohydrodynamic instability of a viscoelastic liquid sheet of Rivlin-Ericksen type that is running between two dielectric gas streams with nonzero identical velocities. To the best of my knowledge, this issue hasn't yet been looked into. In order to demonstrate the impact of different parameters on the stability of both cases in two and three dimensional cases, two dispersion relations have been constructed in sophisticated forms for both cases of antisymmetric and symmetric disturbance. These relations are then numerically solved. The structure of this essay is as follows: The theoretical model and its governing equations are described in section 2. The required boundary conditions for disturbances are provided in Section 3. The solutions to the symmetric and antisymmetric disturbances for the gas and liquid media with an applied electric field are shown in Sections 4 and 5, respectively. The detailed derivation of the analytical dimensionless dispersion relations between wave number and temporal growth rate is covered in Section 6. In sections 7 (two and three dimensions), the dispersion relations are numerically solved, and the impacts of all physical parameters on the temporal growth rate are discussed. The key conclusions and the numerical method employed in this study are summarized in Sections 8 and 9, respectively.

2. Formulation of the problem and perturbation equations

We investigate a viscoelastic Rivlin-Ericksen type dielectric liquid sheet whose thickness is $2a$ that issues from a nozzle at a velocity U_{0l} and has a density ρ_l, pressure p_l, dielectric constant ε_l, kinematic viscosity $\nu_l(=\mu_l/\rho_l)$ and kinematic viscoelasticity $\nu_l'(=\mu_l'/\rho_l)$, where μ_l and μ_l' are the dynamic viscosity and dynamic viscoelasticity, respectively. The liquid sheet is streaming through an inviscid dielectric gas whose velocity is U_{0g}, and has a density ρ_g, pressure p_g, dielectric constant ε_g in the presence of a horizontal electric field E_0 moving parallel to the interfaces $y=\pm a$.The following definitions are given in three-dimensional cartesian coordinates for the equation of continuity and the Navier-Stokes equations for both liquid and gas media.

$$\frac{\partial u_l}{\partial x}+\frac{\partial v_l}{\partial y}+\frac{\partial w_l}{\partial z}=0 \tag{1}$$

$$\frac{\partial u_l}{\partial t}+u_l\frac{\partial u_l}{\partial x}+v_l\frac{\partial u_l}{\partial y}+w_l\frac{\partial u_l}{\partial z}=-\frac{1}{\rho_l}\frac{\partial p_l}{\partial x}+\left(\nu_l+\nu_l'\frac{\partial}{\partial t}\right)\nabla^2 u_{1l} \tag{2}$$

$$\frac{\partial v_l}{\partial t}+u_l\frac{\partial v_l}{\partial x}+v_l\frac{\partial v_l}{\partial y}+w_l\frac{\partial v_l}{\partial z}=-\frac{1}{\rho_l}\frac{\partial p_l}{\partial y}+\left(\nu_l+\nu_l'\frac{\partial}{\partial t}\right)\nabla^2 v_{1l} \tag{3}$$

$$\frac{\partial w_l}{\partial t}+u_l\frac{\partial w_l}{\partial x}+v_l\frac{\partial w_l}{\partial y}+w_l\frac{\partial w_l}{\partial z}=-\frac{1}{\rho_l}\frac{\partial p_l}{\partial z}+\left(\nu_l+\nu_l'\frac{\partial}{\partial t}\right)\nabla^2 w_{1l} \tag{4}$$

$$\frac{\partial u_g}{\partial x}+\frac{\partial v_g}{\partial y}+\frac{\partial w_g}{\partial z}=0 \tag{5}$$

$$\frac{\partial u_g}{\partial t}+u_g\frac{\partial u_g}{\partial x}+v_g\frac{\partial u_g}{\partial y}+w_g\frac{\partial u_g}{\partial z} = -\frac{1}{\rho_g}\frac{\partial p_g}{\partial x} \tag{6}$$

$$\frac{\partial v_g}{\partial t}+u_g\frac{\partial v_g}{\partial x}+v_g\frac{\partial v_g}{\partial y}+w_g\frac{\partial v_g}{\partial z} = -\frac{1}{\rho_g}\frac{\partial p_g}{\partial y} \tag{7}$$

$$\frac{\partial w_g}{\partial t}+u_g\frac{\partial w_g}{\partial x}+v_g\frac{\partial w_g}{\partial y}+w_g\frac{\partial w_g}{\partial z} = -\frac{1}{\rho_g}\frac{\partial p_g}{\partial z} \tag{8}$$

We presum that this problem can be accurately approximated by the quasi-static approximation, then the applied electric field $\mathbf{E}$ can be derived from the gradient of a scalar potential ψ, and so, the linearized Maxwell's equations that govern the electric field become [12]

$$\nabla\cdot\left(\varepsilon_j\mathbf{E}_j\right) = 0 \tag{9}$$

$$\nabla\times\mathbf{E}_j = 0, \tag{10}$$

where the subscript $\left(j=l\right)$ denotes the liquid sheet, while the subscript $\left(j=g\right)$ denotes the gas medium so that the total electric field is given by

$$\mathbf{E}_j=E_0\mathbf{i}-\nabla\psi_j \tag{11}$$

where $\mathbf{i}$ is the unit vector in the x-direction. From equations (9)-(11) we find that the electric potentials in the two regions satisfy Laplace's equations

$$\nabla^2\psi_j=0 \tag{12}$$

The flow has been separated into a time-dependent disturbance and a stable basic flow. Let $u_{1j},v_{1j},w_{1j},p_{1j}$ and ψ_{1j}, where $(j=l,g)$ in the liquid and gas media, denote the perturbation in fluid velocity components u_j,v_j,w_j, the pressure p_j and the electric potentials ψ_j. Hence, we can write

$$u_j=U_{0j}+u_{1j},\ v_j=v_{1j},\ w_j=w_{1j},\ p_j=p_{0j}+p_{1j} \text{ and } \psi_j=\psi_{0j}+\psi_{1j}$$

Substitute into eqs. (1)-(8) and (12) we obtain in the liquid sheet medium, the perturbed equations in the form

$$\frac{\partial u_{1l}}{\partial x}+\frac{\partial v_{1l}}{\partial y}+\frac{\partial w_{1l}}{\partial z}=0 \tag{13}$$

$$\frac{\partial u_{1l}}{\partial t}+U_{0l}\frac{\partial u_{1l}}{\partial x}=-\frac{1}{\rho_l}\frac{\partial p_{1l}}{\partial x}+\left(\nu_l+\nu_l'\frac{\partial}{\partial t}\right)\nabla^2 u_{1l} \tag{14}$$

$$\frac{\partial v_{1l}}{\partial t}+U_{0l}\frac{\partial v_{1l}}{\partial x}=-\frac{1}{\rho_l}\frac{\partial p_{1l}}{\partial y}+\left(\nu_l+\nu_l'\frac{\partial}{\partial t}\right)\nabla^2 v_{1l} \tag{15}$$

$$\frac{\partial w_{1l}}{\partial t}+U_{0l}\frac{\partial w_{1l}}{\partial x}=-\frac{1}{\rho_l}\frac{\partial p_{1l}}{\partial z}+\left(\nu_l+\nu_l'\frac{\partial}{\partial t}\right)\nabla^2 w_{1l} \tag{16}$$

and in the gas region as

$$\frac{\partial u_{1g}}{\partial x}+\frac{\partial v_{1g}}{\partial y}+\frac{\partial w_{1g}}{\partial z}=0 \tag{17}$$

$$\frac{\partial u_{1g}}{\partial t}+U_{0g}\frac{\partial u_{1g}}{\partial x} = -\frac{1}{\rho_g}\frac{\partial p_{1g}}{\partial x} \tag{18}$$

$$\frac{\partial v_{1g}}{\partial t}+U_{0g}\frac{\partial v_{1g}}{\partial x} = -\frac{1}{\rho_g}\frac{\partial p_{1g}}{\partial y} \tag{19}$$

$$\frac{\partial w_{1g}}{\partial t}+U_{0g}\frac{\partial w_{1g}}{\partial x} = -\frac{1}{\rho_g}\frac{\partial p_{1g}}{\partial z} \tag{20}$$

and that the perturbed electric potentials in the liquid and gas media are

$$\nabla^2\psi_{1j}=0 \tag{21}$$

3. Normal modes analysis

To break down the disturbance into its component normal modes, we seek solution of equations (13)-(21), for the liquid and gas media, whose dependence on x, y, z, and t are of the forms [30]

$$\left(u_{1l}, v_{1l}, w_{1l}, p_{1l}, \psi_{1l}\right) = \left(U_l, V_l, W_l, P_l, \Psi_l\right) \exp\left[i\left(kx + nz\right) + \omega t\right] \tag{22}$$

$$\left(u_{1g}, v_{1g}, w_{1g}, p_{1g}, \psi_{1g}\right) = \left(U_g, V_g, W_g, P_g, \Psi_g\right) \exp\left[i\left(kx + nz\right) + \omega t\right] \tag{23}$$

where U_l,V_l,W_l,P_l,Ψ_l,U_g,V_g,W_g ,P_g and Ψ_g are functions of y only; k and n are the wave numbers in the x and z directions, respectively, and $\omega = \omega_r + i\omega_i$ is the complex frequency, respectively. The real part ω_r represents the rate of growth or decay of the disturbance. depending on whether ω_r is positive or negative, respectively. The imaginary variable ω_i is 2π times the disturbance frequence. The interface displacement is given by [31]

$$\eta = \eta_0 \exp\left[i\left(kx + nz\right) + \omega t\right] \tag{24}$$

Substituting from eqs.(22) and (23) into eqs.(13)-(21), we obtain in the electrified liquid sheet medium the equations

$$ikU_l + DV_l + inW_l = 0 \tag{25}$$

$$\left(\omega + ikU_{0l}\right) U_l = -\frac{ik}{\rho_l} P_l + \left(\nu_l + \nu_l' \frac{\partial}{\partial t}\right)\left(D^2 - m^2\right) U_l \tag{26}$$

$$\left(\omega + ikU_{0l}\right) V_l = -\frac{DP_l}{\rho_l} + \left(\nu_l + \nu_l' \frac{\partial}{\partial t}\right)\left(D^2 - m^2\right) V_l \tag{27}$$

$$\left(\omega + ikU_{0l}\right) W_l = -\frac{in}{\rho_l} P_l + \left(\nu_l + \nu_l' \frac{\partial}{\partial t}\right)\left(D^2 - m^2\right) W_l \tag{28}$$

$$\left(D^2 - m^2\right)\Psi_l = 0 \tag{29}$$

where $D = d/dy$ and $m^2 = k^2 + n^2$, and in the electrified gas medium, we obtain the equations

$$ikU_g + DV_g + inW_g = 0 \tag{30}$$

$$\left(\omega + ikU_{0g}\right) U_g = -\frac{ik}{\rho_g} P_g \tag{31}$$

$$\left(\omega + ikU_{0g}\right) V_g = -\frac{DP_g}{\rho_g} \tag{32}$$

$$\left(\omega + ikU_{0g}\right) W_g = -\frac{in}{\rho_g} P_g \tag{33}$$

$$\left(D^2 - m^2\right)\Psi_g = 0 \tag{34}$$

The solutions of eqs. (29) and (34) can be written in the form

$$\left(\Psi_l, \Psi_g\right) = \left(A_1, B_1\right) e^{my} + \left(A_2, B_2\right) e^{-my} \tag{35}$$

Hence

$$\Psi_g = B_1 e^{my} \;\; for \;\; y \le -a \;\; \text{and} \;\; \Psi_g = B_2 e^{-my} \;\; for \;\; y \ge a \;\; \text{since} \; \Psi_g \to 0 \;\; \text{as} \;\; y \to \pm\infty \tag{36}$$

where A_1, A_2, B_1, and B_2 are constants to be determined, using the boundary conditions.

Multiplying eq. (26) by ik, operate by the operator D on eq. (27), and multiply eq. (28) by in, and adding the resulting three equations and using eq. (25), we obtain

$$\left(D^2 - m^2\right) P_l = 0 \tag{37}$$

The solution of eq. (37) is given by

$$P_l = C_1 e^{my} + C_2 e^{-my} \tag{38}$$

where C_1 and C_2 are constants of integration to be determined, equation (26) on using eq. (38) can be written in the form

$$\frac{d^2U_l}{dy^2} - s^2U_l = \frac{ik(C_1e^{my} + C_2e^{-my})}{\rho_l\left(\nu_l + \nu_l'\omega\right)} \tag{39}$$

where

$$s^2 = m^2 + \frac{(\omega + ikU_{0l})}{\left(\nu_l + \nu_l'\omega\right)} \tag{40}$$

Similarly, eqs. (27) and (28) can be written on using eq. (38) in the forms

$$\frac{d^2V_l}{dy^2} - s^2V_l = \frac{m(C_1e^{my} - C_2e^{-my})}{\rho_l\left(\nu_l + \nu_l'\omega\right)} \tag{41}$$

$$\frac{d^2W_l}{dy^2} - s^2W_l = \frac{in(C_1e^{my} + C_2e^{-my})}{\rho_l\left(\nu_l + \nu_l'\omega\right)} \tag{42}$$

The general solution of the non-homogeneous eq. (39) is

$$U_l = C_3e^{sy} + C_4e^{-sy} + \frac{ik}{\rho_l\left(\nu_l + \nu_l'\omega\right)}\frac{(C_1e^{my} + C_2e^{-my})}{\left(m^2 - s^2\right)} \tag{43}$$

Similarly, the general solutions of eqs. (41) and (42) are

$$V_l = C_5e^{sy} + C_6e^{-sy} + \frac{m}{\rho_l\left(\nu_l + \nu_l'\omega\right)}\frac{(C_1e^{my} - C_2e^{-my})}{\left(m^2 - s^2\right)} \tag{44}$$

$$W_l = C_7e^{sy} + C_8e^{-sy} + \frac{in}{\rho_l\left(\nu_l + \nu_l'\omega\right)}\frac{(C_1e^{my} + C_2e^{-my})}{\left(m^2 - s^2\right)} \tag{45}$$

Also, multiplying eq. (31) by ik, operate by the operator D on eq. (32), and multiply eq. (33) by in, and adding the resulting three equations and using eq. (30), we obtain

$$\left(D^2 - m^2\right)P_g = 0 \tag{46}$$

The solution of eq. (46) is

$$P_g = C_9e^{my} + C_{10}e^{-my} \tag{47}$$

where C_9 and C_{10} are constants of integration to be determined.

4. Boundary conditions

Depending on whether the obtained disturbance is symmetric or antisymmetric, different boundary conditions must be used for this problem. For antisymmetric disturbance, the upper andm lower interfaces at $y \approx \pm a$ is described, respectively, by $y = a + \eta$ and $y = -a + \eta$, have the following form, while for symmetric disturbance, the two interfaces are described, respectively, by $y = a + \eta$ and $y = -a - \eta$, where η is the interface displacement defined by equation (24). The linearized boundary conditions for the antisymmetric disturbances at $y \approx \pm a$ are [32, 33]

(1) The normal velocity at the interfaces should equal the total derivative of the interface displacement in order to satisfy the kinematic boundary condition.

$$v_{1l} = \frac{\partial\eta}{\partial t} + U_{0l}\frac{\partial\eta}{\partial x} \text{ at } y \approx \pm a \tag{48}$$

$$v_{1g} = \frac{\partial\eta}{\partial t} + U_{0g}\frac{\partial\eta}{\partial x} \text{ at } y \approx \pm a \tag{49}$$

(2) Far from the interfaces, the perturbed gas velocity should vanish, so

$$v_{1g} = 0 \text{ at } y \to \pm\infty \tag{50}$$

(3) At the interfaces, the stress tensor's tangential component ought to be continuous [23]

$$\tau_{yx}=\left(\mu_l+\mu_l^{'}\frac{\partial}{\partial t}\right)\left(\frac{\partial u_{1l}}{\partial y}+\frac{\partial v_{1l}}{\partial x}\right)=0 \text{ at } y\approx\pm a \tag{51}$$

$$\tau_{yz}=\left(\mu_l+\mu_l^{'}\frac{\partial}{\partial t}\right)\left(\frac{\partial v_{1l}}{\partial z}+\frac{\partial w_{1l}}{\partial y}\right)=0 \text{ at } y\approx\pm a \tag{52}$$

(4) At the interfaces, the electric field's tangential component is continuous, i.e.

$$\frac{\partial\psi_{1l}}{\partial x}=\frac{\partial\psi_{1g}}{\partial x} \text{ at } y\approx\pm a \tag{53}$$

(5) At the interfaces, the electric displacement's normal component is continuous.

$$\varepsilon_l\frac{\partial\psi_{1l}}{\partial y}-\varepsilon_g\frac{\partial\psi_{1g}}{\partial y}=ik\eta_0E_0\left(\varepsilon_l-\varepsilon_g\right) \text{ at } y\approx\pm a \tag{54}$$

(6) Surface tension causes the normal component of the stress tensor to discontinue at interfaces [34, 35]

$$-p_{1l}+\varepsilon_lE_0\frac{\partial\psi_{1l}}{\partial x}+2\left(\mu_l+\mu_l^{'}\frac{\partial}{\partial t}\right)\frac{\partial v_{1l}}{\partial y}=-p_{1g}+\varepsilon_gE_0\frac{\partial\psi_{1g}}{\partial x}+p_\sigma \text{ at } y\approx\pm a \tag{55}$$

where p_σ is the pressure induced by the surface tension σ.

Note that, for symmetric disturbances, the boundary conditions that change forms are the kinematic boundary conditions (48), (49) at $y=-a$ which become

$$v_{1l}=-\left(\frac{\partial\eta}{\partial t}+U_{0l}\frac{\partial\eta}{\partial x}\right) \text{ at } y\approx-a \tag{56}$$

$$v_{1g}=-\left(\frac{\partial\eta}{\partial t}+U_{0g}\frac{\partial\eta}{\partial x}\right) \text{ at } y\approx-a \tag{57}$$

and the electric displacement boundary condition (54) which becomes [36]

$$\varepsilon_l\frac{\partial\psi_{1l}}{\partial y}-\varepsilon_g\frac{\partial\psi_{1g}}{\partial y}=-ik\eta_0E_0\left(\varepsilon_l-\varepsilon_g\right) \text{ at } y\approx-a \tag{58}$$

5. Solutions for the antisymmetric disturbances

5.1. Solution of the electric field

Substituting for ψ_{1l} and ψ_{1g} from eqs. (22), (23), (35) and (36) into the boundary condition (53) and (54), we obtain

$$A_1e^{ma}+A_2e^{-ma}=B_2e^{-ma} \tag{59}$$

$$A_1e^{-ma}+A_2e^{ma}=B_1e^{-ma} \tag{60}$$

$$\varepsilon_lm(A_1e^{ma}-A_2e^{-ma})+\varepsilon_gmB_2e^{-ma}=ik\eta_0E_0(\varepsilon_l-\varepsilon_g) \tag{61}$$

$$\varepsilon_lm(A_1e^{-ma}-A_2e^{ma})-\varepsilon_gmB_1e^{-ma}=ik\eta_0E_0(\varepsilon_l-\varepsilon_g) \tag{62}$$

solving eqs. (59)-(62), we obtain

$$B_1=-B_2=-\frac{ik\eta_0E_0(\varepsilon_l-\varepsilon_g)e^{ma}\tanh(ma)}{m[\varepsilon_l+\varepsilon_g\tanh(ma)]} \tag{63}$$

and

$$A_1=-A_2=\frac{ik\eta_0E_0(\varepsilon_l-\varepsilon_g)}{2m\cosh(ma)[\varepsilon_l+\varepsilon_g\tanh(ma)]} \tag{64}$$

Then, the electric potential in both regions can be written in the form

$$\psi_{1l}=\frac{ik\eta_0E_0(\varepsilon_l-\varepsilon_g)\sinh(my)}{m\cosh(ma)[\varepsilon_l+\varepsilon_g\tanh(ma)]}e^{i(kx+nz)+\omega t} \tag{65}$$

$$\psi_{1g}^{u,l}=\pm\frac{ik\eta_0E_0(\varepsilon_l-\varepsilon_g)e^{m(a\mp y)}\tanh(ma)}{m[\varepsilon_l+\varepsilon_g\tanh(ma)]}\tanh(ma)e^{i(kx+nz)+\omega t} \tag{66}$$

5.2. Solution of the liquid sheet phase

The boundary conditions (48), (51), (52), on using eqs. (22), (24), (43), (44), (67) and (68), yield the following solutions

$$C_3 = -\frac{ikm\{C_1\sinh[(s+m)a] - C_2\sinh[(s-m)a]\}}{s\rho_l\left(\nu_l+\nu_l'\omega\right)\left(m^2-s^2\right)\sinh(2sa)} - \frac{ik(\omega+ikU_{0l})\eta_0}{2s\cosh(sa)} \tag{67}$$

$$C_4 = \frac{ikm\{C_1\sinh[(s-m)a] - C_2\sinh[(s+m)a]\}}{s\rho_l\left(\nu_l+\nu_l'\omega\right)\left(m^2-s^2\right)\sinh(2sa)} + \frac{ik(\omega+ikU_{0l})\eta_0}{2s\cosh(sa)} \tag{68}$$

$$C_5 = -\frac{m\{C_1\sinh[(s+m)a] - C_2\sinh[(s-m)a]\}}{\rho_l\left(\nu_l+\nu_l'\omega\right)\left(m^2-s^2\right)\sinh(2sa)} + \frac{(\omega+ikU_{0l})\eta_0}{2\cosh(sa)} \tag{69}$$

$$C_6 = -\frac{m\{C_1\sinh[(s-m)a] - C_2\sinh[(s+m)a]\}}{\rho_l\left(\nu_l+\nu_l'\omega\right)\left(m^2-s^2\right)\sinh(2sa)} + \frac{(\omega+ikU_{0l})\eta_0}{2\cosh(sa)} \tag{70}$$

$$C_7 = -\frac{inm\{C_1\sinh[(s+m)a] - C_2\sinh[(s-m)a]\}}{s\rho_l\left(\nu_l+\nu_l'\omega\right)\left(m^2-s^2\right)\sinh(2sa)} - \frac{in(\omega+ikU_{0l})\eta_0}{2s\cosh(sa)} \tag{71}$$

$$C_8 = \frac{inm\{C_1\sinh[(s-m)a] - C_2\sinh[(s+m)a]\}}{s\rho_l\left(\nu_l+\nu_l'\omega\right)\left(m^2-s^2\right)\sinh(2sa)} + \frac{in(\omega+ikU_{0l})\eta_0}{2s\cosh(sa)} \tag{72}$$

Since the equation of continuity (13) is satisfied everywhere in the liquid sheet, it is also satisfied at the two interfaces. Hence, on using eqs. (67)-(72), it reduces to

$$\begin{aligned}&\frac{m}{s\rho_l(\nu_l+\nu'_l\omega)\sinh(sa)\cosh(sa)}\times\\&\left\{\left[\sinh^2(sa)\cosh(ma)+\cosh^2(sa)\sinh(ma)\right]C_1+\left[-\sinh^2(sa)\cosh(ma)+\cosh^2(sa)\sinh(ma)\right]C_2\right\}\\&\qquad+\frac{(\omega+ikU_{0l})\eta_0}{s\cosh(sa)}\left(m^2+s^2\right)\sinh(sa)=0\end{aligned} \tag{73}$$

and

$$\begin{aligned}&\frac{m}{s\rho_l(\nu_l+\nu'_l\omega)\sinh(sa)\cosh(sa)}\times\\&\left\{\left[-\sinh^2(sa)\cosh(ma)+\cosh^2(sa)\sinh(ma)\right]C_1+\left[\sinh^2(sa)\cosh(ma)+\cosh^2(sa)\sinh(ma)\right]C_2\right\}\\&\qquad-\frac{(\omega+ikU_{0l})\eta_0}{s\cosh(sa)}\left(m^2+s^2\right)\sinh(sa)=0\end{aligned} \tag{74}$$

Solving eqs. (73) and (74), we obtain

$$C_1 = -C_2 = -\frac{\rho_l\left(\nu_l+\nu_l'\omega\right)\left(m^2+s^2\right)(\omega+ikU_{0l})\eta_0}{2m\cosh(ma)} \tag{75}$$

Substituting for C_1 and C_2 into eqs. (67)-(72), and using the fact that $(\omega+ikU_{0l}) = \left(s^2-m^2\right)\left(\nu_l+\nu_l'\omega\right)$, we respectively obtain

$$C_3 = -C_4 = -\frac{iks\left(\nu_l+\nu_l'\omega\right)\eta_0}{\cosh(sa)} \tag{76}$$

$$C_5 = C_6 = -\frac{m^2\left(\nu_l+\nu_l'\omega\right)\eta_0}{\cosh(sa)} \tag{77}$$

$$C_7 = -C_8 = -\frac{ins\left(\nu_l+\nu_l'\omega\right)\eta_0}{\cosh(sa)} \tag{78}$$

Hence, we have the following solutions for the liquid phase

$$p_{1l} = -\frac{\rho_l}{m}\left(\nu_l+\nu_l'\omega\right)\left(m^2+s^2\right)(\omega+ikU_{0l})\eta_0\frac{\sinh(my)}{\cosh(ma)} \times \exp\left[i\left(kx+nz\right)+\omega t\right] \tag{79}$$

$$u_{1l} = -ik\eta_0\left[2s\left(\nu_l+\nu_l'\omega\right)\frac{\sinh(sy)}{\cosh(sa)}+\frac{\left(m^2+s^2\right)(\omega+ikU_{0l})}{m\left(m^2-s^2\right)}\frac{\sinh(my)}{\cosh(ma)}\right] \times \exp\left[i\left(kx+nz\right)+\omega t\right] \tag{80}$$

$$v_{1l} = -\eta_0\left[2m^2\left(\nu_l+\nu_l'\omega\right)\frac{\cosh(sy)}{\cosh(sa)}+\frac{\left(m^2+s^2\right)(\omega+ikU_{0l})}{\left(m^2-s^2\right)}\frac{\cosh(my)}{\cosh(ma)}\right] \times \exp\left[i\left(kx+nz\right)+\omega t\right] \tag{81}$$

$$w_{1l} = -in\eta_0\left[2s\left(\nu_l+\nu_l'\omega\right)\frac{\sinh(sy)}{\cosh(sa)}+\frac{\left(m^2+s^2\right)(\omega+ikU_{0l})}{m\left(m^2-s^2\right)}\frac{\sinh(my)}{\cosh(ma)}\right] \times \exp\left[i\left(kx+nz\right)+\omega t\right] \tag{82}$$

5.3. Solution in the gas phase

Substitute from eqs. (47) into eqs. (31)-(33), we get

$$U_g = -\frac{ik\left[C_9e^{my}+C_{10}e^{-my}\right]}{\rho_g\left(\omega+ikU_{0g}\right)} \tag{83}$$

$$V_g = -\frac{m\left[C_9e^{my}-C_{10}e^{-my}\right]}{\rho_g\left(\omega+ikU_{0g}\right)} \tag{84}$$

$$W_g = -\frac{in\left[C_9e^{my}+C_{10}e^{-my}\right]}{\rho_g\left(\omega+ikU_{0g}\right)} \tag{85}$$

using the kinematic boundary condition for the gas medium (49), we get

$$C_9e^{my}-C_{10}e^{-my} = -\frac{\rho_g\left(\omega+ikU_{0g}\right)^2\eta_0}{m} \quad \text{at} \quad y\approx\pm a \tag{86}$$

From the boundary condition (50) it follows that $C_9=0$ due to $v_{1g}=0$ as $y\to\infty$, then

$$C_{10} = \frac{\rho_g\left(\omega+ikU_{0g}\right)^2\eta_0}{m}e^{ma}, \quad y>a \tag{87}$$

while $C_{10}=0$ due to $v_{1g}=0$ as $y\to-\infty$, then

$$C_9 = -\frac{\rho_g\left(\omega+ikU_{0g}\right)^2\eta_0}{m}e^{ma}, \quad y<-a \tag{88}$$

Substitute from eqs. (87) and (88) into eqs. (83)-(85), and using eqs. (23) and (47), we get the velocity and pressure disturbances in the gas medium, for the regions $y>a$ and $y<-a$ as follows

$$p_{1g} = \pm\frac{\rho_g\left(\omega+ikU_{0g}\right)^2\eta_0}{m}e^{m(a\mp y)}\exp\left[i\left(kx+nz\right)+\omega t\right] \tag{89}$$

$$u_{1g} = \mp\frac{ik\left(\omega+ikU_{0g}\right)\eta_0}{m}e^{m(a\mp y)}\exp\left[i\left(kx+nz\right)+\omega t\right] \tag{90}$$

$$v_{1g} = (\omega+ikU_{0g})\eta_o e^{m(a\mp y)}\exp\left[i\left(kx+nz\right)+\omega t\right] \tag{91}$$

$$w_{1g} = \mp\frac{in\left(\omega+ikU_{0g}\right)\eta_0}{m}e^{m(a\mp y)}\exp\left[i\left(kx+nz\right)+\omega t\right] \tag{92}$$

A definition of the pressure caused by surface tension by [31]

$$p_\sigma = \sigma\left(\frac{\partial^2\eta}{\partial x^2}+\frac{\partial^2\eta}{\partial z^2}\right) = -m^2\sigma\eta_0\exp\left[i\left(kx+nz\right)+\omega t\right] \tag{93}$$

6. Solutions for the symmetric disturbances

6.1. Solution of the electric field

Substituting for ψ_{1l} and ψ_{1g} from eqs. (22),(23),(35), and (36) into the boundary condition (53) at $y = \pm a$, (54) at $y = a$, and (58) at $y = -a$, we obtain the same eqs. (59)-(61) obtained before, but equation (62) is replaced by the equation

$$\varepsilon_l m(A_1 e^{-ma} - A_2 e^{ma}) - \varepsilon_g m B_1 e^{-ma} = -ik\eta_0 E_0(\varepsilon_l - \varepsilon_g) \tag{94}$$

then solving these equations, we get

$$B_1 = B_2 = \frac{ik\eta_0 E_0(\varepsilon_l - \varepsilon_g) e^{ma} \coth(ma)}{m[\varepsilon_l + \varepsilon_g \coth(ma)]} \tag{95}$$

and

$$A_1 = A_2 = \frac{ik\eta_0 E_0(\varepsilon_l - \varepsilon_g)}{2m \sinh(ma)[\varepsilon_l + \varepsilon_g \coth(ma)]} \tag{96}$$

Therefore, we have the solutions of the electric potentials as

$$\psi_{1l} = \frac{ik\eta_0 E_0(\varepsilon_l - \varepsilon_g)\cosh(my)}{m \sinh(ma)[\varepsilon_l + \varepsilon_g \coth(ma)]} e^{i(kx+nz)+\omega t} \tag{97}$$

and

$$\psi_{1g}^{u,l} = \frac{ik\eta_0 E_0(\varepsilon_l - \varepsilon_g) e^{m(a\mp y)} \coth(ma)}{m[\varepsilon_l + \varepsilon_g \coth(ma)]} \coth(ma) e^{i(kx+nz)+\omega t} \tag{98}$$

6.2. Solution of the liquid sheet phase

As a result, we continue in a manner identical to that of the prior antisymmetric disturbance instance except that the kinematic boundary condition (48) is applied at the interface $y = a$, while at the lower interface $y = -a$, we use the condition (56), and also apply the boundary conditions (51) and (52) to obtain the following constants of integration

$$C_1 = C_2 = -\frac{\rho_l \left(\nu_l + \nu_l' \omega\right)\left(m^2 + s^2\right)(\omega + ikU_0)\eta_0}{2m \sinh(ma)} \tag{99}$$

$$C_3 = C_4 = -\frac{iks\left(\nu_l + \nu_l' \omega\right)\eta_0}{\sinh(sa)} \tag{100}$$

$$C_5 = -C_6 = -\frac{m^2\left(\nu_l + \nu_l' \omega\right)\eta_0}{\sinh(sa)} \tag{101}$$

$$C_7 = C_8 = -\frac{ins\left(\nu_l + \nu_l' \omega\right)\eta_0}{\sinh(sa)} \tag{102}$$

Hence, we have the following solutions for the liquid phase

$$\begin{aligned} p_{1l} &= -\frac{\rho_l}{m}\left(\nu_l + \nu_l' \omega\right)\left(m^2 + s^2\right)(\omega + ikU_{0l})\eta_0 \frac{\cosh(my)}{\sinh(ma)} \\ &\quad \times \exp[i(kx + nz) + \omega t] \end{aligned} \tag{103}$$

$$\begin{aligned} u_{1l} &= -ik\eta_0 \left[2s\left(\nu_l + \nu_l' \omega\right)\frac{\cosh(sy)}{\sinh(sa)} + \frac{\left(m^2 + s^2\right)(\omega + ikU_{0l})}{m\left(m^2 - s^2\right)}\frac{\cosh(my)}{\sinh(ma)}\right] \\ &\quad \times \exp[i(kx + nz) + \omega t] \end{aligned} \tag{104}$$

$$\begin{aligned} v_{1l} &= -\eta_0 \left[2m^2\left(\nu_l + \nu_l' \omega\right)\frac{\sinh(sy)}{\sinh(sa)} + \frac{\left(m^2 + s^2\right)(\omega + ikU_{0l})}{\left(m^2 - s^2\right)}\frac{\sinh(my)}{\sinh(ma)}\right] \\ &\quad \times \exp[i(kx + nz) + \omega t] \end{aligned} \tag{105}$$

$$\begin{aligned} w_{1l} &= -in\eta_0 \left[2s\left(\nu_l + \nu_l' \omega\right)\frac{\cosh(sy)}{\sinh(sa)} + \frac{\left(m^2 + s^2\right)(\omega + ikU_{0l})}{m\left(m^2 - s^2\right)}\frac{\cosh(my)}{\sinh(ma)}\right] \\ &\quad \times \exp[i(kx + nz) + \omega t] \end{aligned} \tag{106}$$

6.3. Solution in the gas phase

Here, we proceed in a similar way to the antisymmetric disturbance case axcept that the kinamatic boundary condition for the gas (49) is satisfied at $y = a$, while at the lower interface $y = -a$, we use the condition (57), then , we get the pressure and velocity components in the gas medium in the regions $y > a$ and $y < -a$ in the form

$$p_{1g} = \frac{\rho_g\left(\omega + ikU_{0g}\right)^2\eta_0}{m}e^{m(a\mp y)}\exp\left[i\left(kx+nz\right)+\omega t\right] \tag{107}$$

$$u_{1g} = -\frac{ik\left(\omega + ikU_{0g}\right)\eta_0}{m}e^{m(a\mp y)}\exp\left[i\left(kx+nz\right)+\omega t\right] \tag{108}$$

$$v_{1g} = \pm(\omega + ikU_{0g})\eta_o e^{m(a\mp y)}\exp\left[i\left(kx+nz\right)+\omega t\right] \tag{109}$$

$$w_{1g} = -\frac{in\left(\omega + ikU_{0g}\right)\eta_0}{m}e^{m(a\mp y)}\exp\left[i\left(kx+nz\right)+\omega t\right] \tag{110}$$

7. Dispersion relations and stability analysis

Substituting from eqs. (65), (66), (79), (81), (89) and (93) into the normal stress boundary condition (55), for $y = a$ leads to dispersion relation between k and ω , for antisymmetric disturbances

$$\begin{aligned}&\left(\nu_l+\nu_l'\omega\right)\left(m^2+s^2\right)\left[\rho_l\left(\omega+ikU_{0l}\right)+2\rho_l m^2\left(\nu_l+\nu_l'\omega\right)\right]\tanh\left(ma\right)\\&-4\rho_l m^3 s\left(\nu_l+\nu_l'\omega\right)^2\tanh\left(sa\right)-\frac{k^2E_0^2(\varepsilon_l-\varepsilon_g)^2}{\left[\varepsilon_l+\varepsilon_g\tanh(ma)\right]}\tanh(ma)\\&+\rho_g\left(\omega+ikU_{0g}\right)^2+m^3\sigma=0\end{aligned} \tag{111}$$

Also, substituting from eqs. (97), (98), (103), (105), (107) and (93) into the boundary condition (55) foe $y = a$, leads to the following dispersion relation for the symmetric disturbance case.

$$\begin{aligned}&\left(\nu_l+\nu_l'\omega\right)\left(m^2+s^2\right)\left[\rho_l\left(\omega+ikU_{0l}\right)+2\rho_l m^2\left(\nu_l+\nu_l'\omega\right)\right]\coth\left(ma\right)\\&-4\rho_l m^3 s\left(\nu_l+\nu_l'\omega\right)^2\coth\left(sa\right)-\frac{k^2E_0^2(\varepsilon_l-\varepsilon_g)^2}{\left[\varepsilon_l+\varepsilon_g\coth(ma)\right]}\coth(ma)\\&+\rho_g\left(\omega+ikU_{0g}\right)^2+m^3\sigma=0\end{aligned} \tag{112}$$

Note that, the dispersion relation for symmetric disturbances is similar to eq. (111) except that $\tanh(ma)$ and $\tanh(sa)$ are replaced by $\coth(ma)$ and $\coth(sa)$, respectively.

To facilitate the analysis, we should write equations (111) and (112) in dimensionless forms using the following non-dimensional quantities: $We = \rho_l U_{0l}^2 a/\sigma$ is the Weber number, $Re = U_{0l}a/\nu_l$ is the Reynolds number, $Oh = \sqrt{We}/Re$ is the Ohnesorge number $\rho = \rho_g/\rho_l$ is the gas to liquid density ratio, $U = U_{0g}/U_{0l}$ is the gas to liquid velocity ratio, $V' = \nu_l'/a^2$ is the viscoelasticity parameter. And let $K = ka$, $N = na$ represent the non-dimensional wave numbers, and put $M = ma$, $S = sa$, $E = E_0/\sqrt{\sigma}$, $\tilde{\varepsilon_l} = \varepsilon_l a$, and $\tilde{\varepsilon_g} = \varepsilon_g a$. Also, we defined the quantities $\Omega = \Omega_r + i\sqrt{We}\Omega_i$ where $\Omega_r = \omega_r a^2\sqrt{\rho_l/\sigma a}$, $\Omega_i = \omega_i a/U_{0l}$ and $\Omega_1 = \Omega + iK\sqrt{We}$.

Then, the non-dimensional form of the dispersion relation (111) can be written, for antisymmetric case, in the form

$$\begin{aligned}&\left[\Omega_1+4M^2(Oh+V'\Omega)\right]\Omega_1\tanh(M)+4M^3(Oh+V'\Omega)^2\left[M\tanh(M)\right.\\&\left.-S\tanh(S)\right]-\frac{K^2E^2(\tilde{\varepsilon_l}-\tilde{\varepsilon_g})^2}{\left[\tilde{\varepsilon_l}+\tilde{\varepsilon_g}\tanh(M)\right]}\tanh(M)+\rho(\Omega+iKU\sqrt{We})^2\\&+M^3=0\end{aligned} \tag{113}$$

where

$$S^2 = M^2 + \frac{\Omega_1}{Oh+\Omega V'} \tag{114}$$

Similarly, the non-dimensional form of the dispersion relation (112) can be written, for symmetric disturbance case, in the form

$$\begin{aligned}&\left[\Omega_1+4M^2(Oh+V'\Omega)\right]\Omega_1\coth(M)+4M^3(Oh+V'\Omega)^2\left[M\coth(M)\right.\\&\left.-S\coth(S)\right]-\frac{K^2E^2(\tilde{\varepsilon_l}-\tilde{\varepsilon_g})^2}{\left[\tilde{\varepsilon_l}+\tilde{\varepsilon_g}\coth(M)\right]}\coth(M)+\rho(\Omega+iKU\sqrt{We})^2\\&+M^3=0\end{aligned} \tag{115}$$

Note that, in absence of both electric field and gas velocity, (i.e. when $E = 0$ and $U = 0$), the dimensionless dispersion relation (113) and (115) reduce to the same dispersion relation obtained before by El.Sayed et al [33], which are generalization of the dispersion relations obtained earlier by Ibrahim and Akpan [37], in absence of the viscoelasticity parameter (i.e. for only viscous fluids, when $V' = 0$), and hence their results are recovered.
The dimensionless dispersion relations (113) and (115) are very complicated, and they cannot be analytically solved in order to investigate the effects of different parameters on the stability of the system under consideration. As a result, they may be using the Mathematica software to solve numerical problems (as shown in the appendix) to yield values of K as a function of Ω for different values of the other parameters. In providing a guessed root of Ω_r, it is helpful to realize that $\Omega_i = -K$ in accordance with Gaster's theorem [38]. Note that, the three-dimensional results are obtained from the numerical solution of the relations (113) and (115) with $N = 1, 2$ (the z-direction wave numbers), while the two-dimensional results corresponds to the case $N = 0$. By solving the dispersion equations (113) and (115) in the temporal mode for both the antisymmetrical and symmetrical disturbances cases, it is possible to examine the effects of different analysis parameters on the instability of an electrified viscoelastic Rivlin-Ericksen liquid sheet. A novel method that combines the Muller method [39] and the Gaster method [38] is used to solve these dispersion relations numerically using Mathematica software, to obtain relationships between the non-dimensional real part of the growth rates Ω_r and the non-dimensional wave numbers K of the disturbances. The physical parameters including in the study are shown graphically in the following figures (1)-(8) which exhibit the growth rate Ω_r as a function of the wave number K for the flow. In these figures, at first Ω_r increases with increasing K and then decreases for both cases of antisymmetrical and symmetrical disturbances. The dominant growth rate is defined as the highest possible value, and the dominant wave number is the corresponding maximum value of the growth rate. The critical wave number is the point where the growth rate curve meets the wave number axis. The Rivlin-Ericksen fluid sheet becomes unstable with positive growth rate in the area under the growth rate curve where the wave number ranges from zero to the cutoff wave number, which is defined as the instability zone. The maximum growth rates Ω_r with the dominant wave number K makes the Rivlin-Ericksen liquid sheet most unstable. Furthermore, the following figures demonstrate that the maximum growth rates of antisymmetrical disturbances are significantly higher than those of symmetrical disturbances, indicating that the antisymmetrical disturbance situation has a greater impact on the Rivlin-Ericksen liquid sheet instability.Therefore, the antisymmetrical disturbances play a major role in the flow instability and breakup of the electrified Rivlin-Ericksen liquid sheet surrounded by an inviscid gas medium [40, 41] .

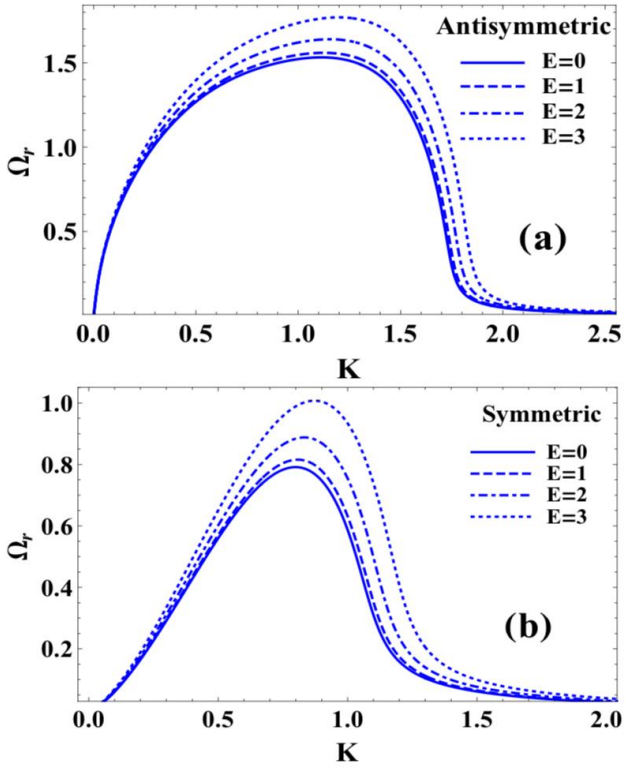

Fig. 1. Variation of growth rate Ω_r with wave number k for various values of electric field E when $We = 10000$, $Oh = 0.1$, $\rho = 0.01$, $N = 0$, $V' = 0.01$, $\tilde{\epsilon_l} = 0.1$, $\tilde{\epsilon_g} = 0.3$ and $U = 1.2$ in (a) antisymmetric and (b) symmetric modes.

7.1. Effect of electric field

Figures 1a,b show the variation of non-dimensional growth rate Ω_r with non-dimensional wave number K for various values of the electric field E, and constant values of the other parameters for both antisymmetrical and symmetrical disturbances, respectively. The instability zone is larger in the antisymmetric case than the symmetric case at any electric field value, even the situation of no electric field, as can be seen from the figure, which shows that the curves of antisymmetrical disturbances are greater than those of symmetrical disturbances. Additionally, we see that as the electric field values rise, the dominating growth rates and related dominant wave numbers rise as well. Therefore, we draw the conclusion that both kinds of disruption are destabilized by the applied electric field.

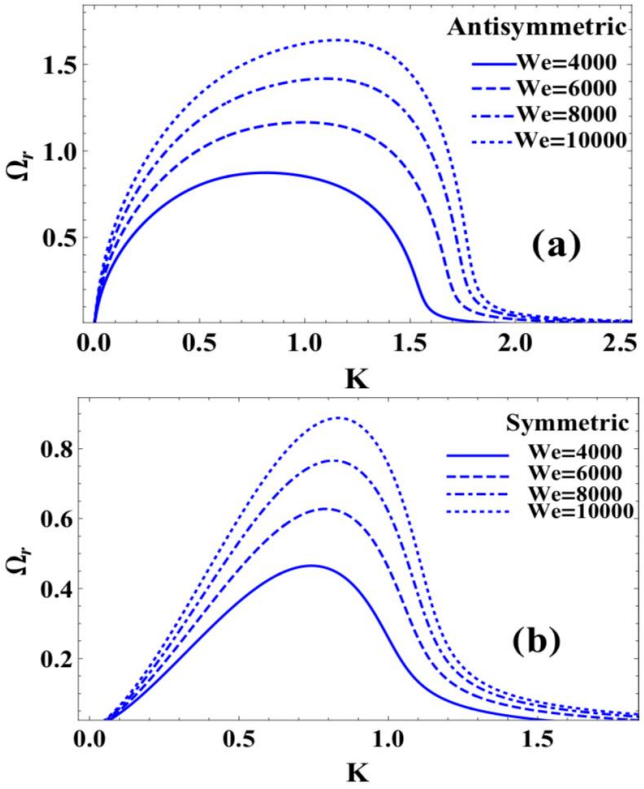

Fig. 2. Variation of growth rate Ω_r with wave number k for various values of Weber number We when $Oh = 0.1$, $\rho = 0.01$, $N = 0$, $V' = 0.01$, $E = 2$, $\tilde{\varepsilon_l} = 0.1$, $\tilde{\varepsilon_g} = 0.3$ and $U = 1.2$ in (a) intisymmetric and (b) symmetric modes.

7.2. Effect of Weber Number

Figures 2a,b give the relation between the non-dimensional growth rate Ω_r and the non-dimensional wave number K for various values of Weber number, We in both cases of antisymmetrical symmetrical modes, respectively, under different initial disturbances.These data show that as the Weber number rises, the dominant wave numbers and dominant growth rates of symmetrical and antisymmetrical modes also rise. As a result, the Weber number both accelerates and reduces the disturbance wavelength in both scenarios. It should be noted that by raising the Weber number faster than their values in the comparable symmetric disturbance case, the maximum growth rates, dominant wave numbers, and critical wave numbers all increase in the antisymmetrical disturbances mode. As a result, we draw the conclusion that the Weber number causes the system to become unstable.

7.3. Effect of viscoelasticity parameter

Figures 3a,b show the variation of non-dimensional growth rates Ω_r with non-dimensional wave number K under different various of viscoelasticity parameter V' for antisymmetrical and symmetrical disturbances, respectively, and constant values of the other parameters included in the analysis. The figure shows that, similar to the aforementioned results, the growth rates of antisymmetrical modes are higher than those of symmetric modes. Additionally, it is seen that for the two disturbance scenarios, growth rates are reduced by raising the viscoelasticity value, and the dominant wave numbers also decrease with the increase of V'. Hence, we conclude that the viscoelasticity parameter V' has a stabilizing effect on the system under consideration, due to the decrease of instability zone.

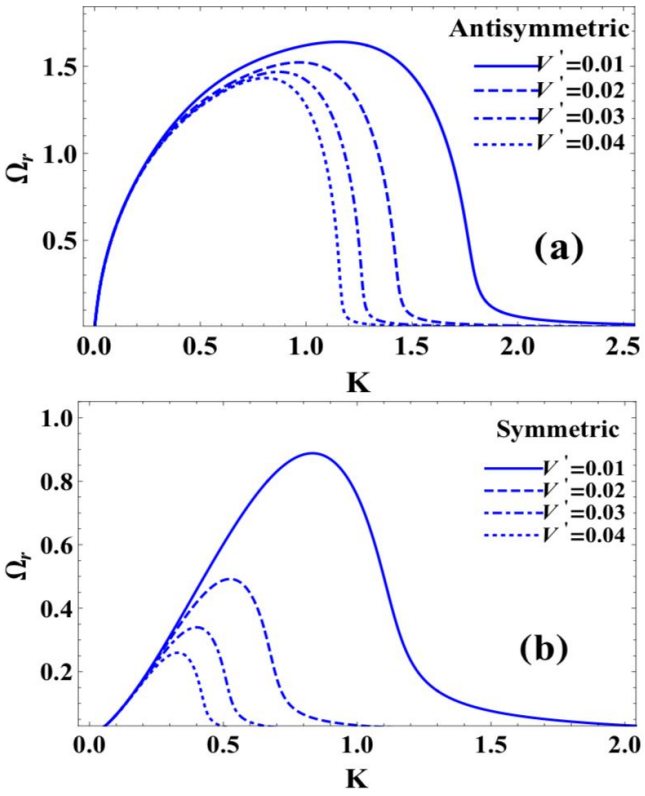

Fig. 3. Variation of growth rate Ω_r with wave number k for various values of viscoelasticity parameter V' when $We = 10000$, $Oh = 0.1$, $\rho = 0.01$, $N = 0$, $E = 2$, $\tilde{\varepsilon_l} = 0.1$, $\tilde{\varepsilon_g} = 0.3$ and $U = 1.2$ in (a) antisymmetric and (b) symmetric modes.

7.4. Effect of Ohnesorge Number

Figures 4a,b show the effect of Ohnesorge number Oh on the non-dimensional growth rate Ω_r and non-dimensional wave number K for antisymmetric and symmetric modes of disturbances, respectively, and the other parameters stay constant. From these figures, it is clear that when the Ohnesorge number Oh is increased the maximum growth rates of antisymmetric and symmetric modes decrease for wave number values less than a fixed wave number value after which both the growth rate and dominant wave number of both modes of disturbance increase. The instability zone in the case of an antisymmetric disturbance is significantly larger than the corresponding instability zone in the case of a symmetric disturbance, leading us to the conclusion that the Ohnesorge number plays a dual role on the stability of the system, stabilizing and then destabilizing effects.

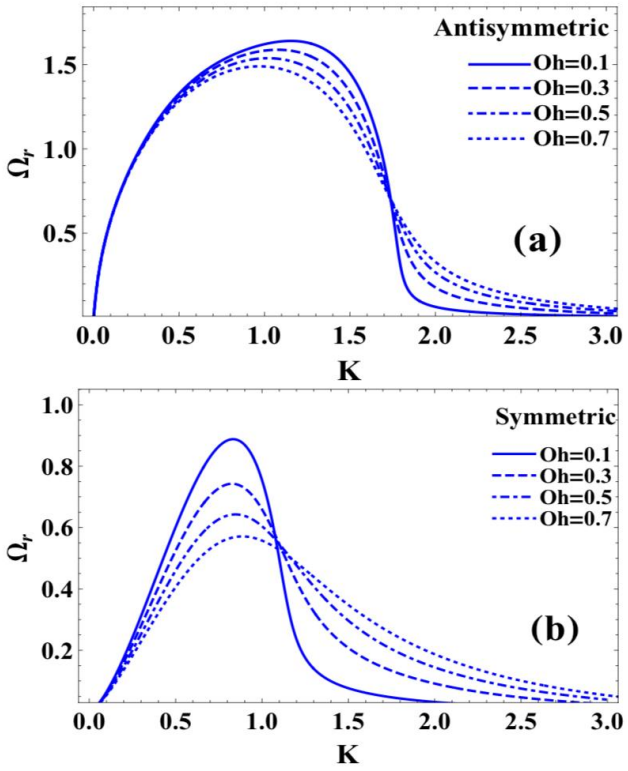

Fig. 4. Variation of growth rate Ω_r with wave number k for various values of Ohnesorge number Oh when $We = 10000$, $\rho = 0.01$, $N = 0$, $V' = 0.01$, $E = 2$, $\bar{\varepsilon_l} = 0.1$, $\bar{\varepsilon_g} = 0.3$ and $U = 1.2$ in (a) antisymmetric, and (b) symmetric modes.

7.5. Effect of gas to liquid density ratio

Figures 5a,b demonstrate the variation of non-dimensional growth rate of disturbance Ω_r with the non-dimensional wave number K under several different values of the gas to liquid density ratio ρ and constant values of the other physical parameters in both antisymmetric and symmetric disturbance modes, respectively,The figure shows that the growth rates and the dominating wave numbers of the symmetric and antisymmetric modes of instability both rise with an increase in the gas to liquid density ratio. This means that in the case of an antisymmetric disturbance, the dominant growth rates, dominant wave numbers, and critical wave numbers are bigger than those in the case of a symmetric disturbance. In all kinds of instability, the disturbance is therefore accelerated by the gas to liquid density ratio. As a result, we draw the conclusion that the system is destabilized by the gas to liquid density ratio, and that this instability occurs more quickly in the antisymmetric mode case than in the comparable symmetric mode situation.

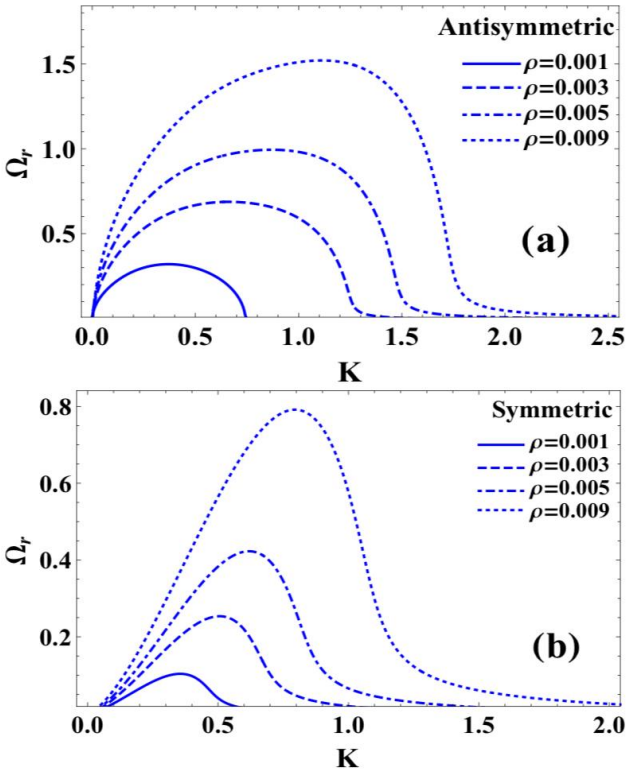

Fig. 5. Variation of growth rate Ω_r with wave number k for various values of gas to liquid density ratio ρ when $We = 10000$, $Oh = 0.1$, $N = 0$, $V' = 0.01$, $E = 2$, $\tilde{\varepsilon_l} = 0.1$, $\tilde{\varepsilon_g} = 0.3$ and $U = 1.2$ in (a) antisymmetric and (b) symmetric modes.

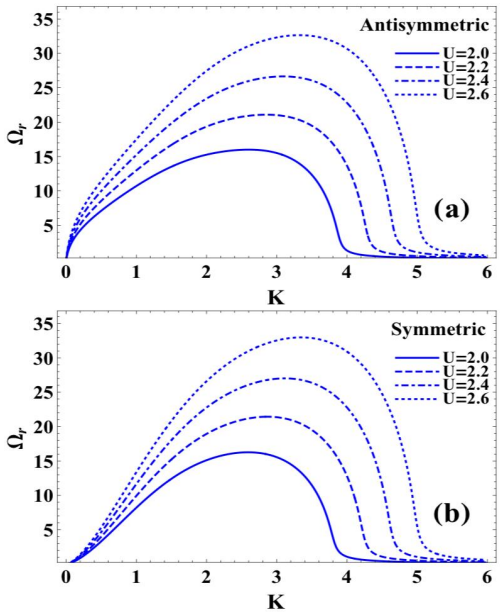

Fig. 6. Variation of growth rate Ω_r with wave number k for various values of gas to liquid velocity ratio $U \geq 2$ when $We = 10000$, $Oh = 0.1$, $\rho = 0.01$, $N = 0$, $V' = 0.01$, $E = 2$, $\tilde{\varepsilon_l} = 0.1$ and $\tilde{\varepsilon_g} = 0.3$ in (a) antisymmetric and (b) symmetric modes.

7.6. Effect of gas to liquid velocity ratio

Figures 6a,b show the effect of the gas to liquid velocity ratio $U \geq 2$ on the instability of Rivlin-Ericksen electrified viscoelastic liquid sheet for both cases of antisymmetrical and symmetrical disturbances, respectively, while Figures 7a,b show the same effect when $0 < U \leq 2$. It is clear from Figures 6a,b that increase the gas to liquid velocity ratio

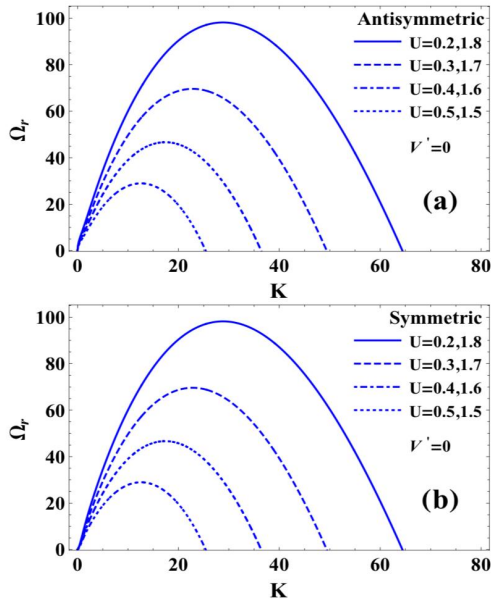

Fig. 7. Variation of growth rate Ω_r with wave number k for various values of gas to liquid velocity ratio $0 < U \leq 2$ when $We = 10000$, $Oh = 0.1$, $\rho = 0.01$, $N = 0$, $E = 2$, $\varepsilon_l = 0.1$ and $\varepsilon_g = 0.3$ in (a) antisymmetric and (b) symmetric modes.

from $U = 2$ to $U = 2.6$, and keeping the other parameters constant, then the growth rates for antisymmetrical and symmetrical disturbances increase, and the dominant growth rates also largely increase with the increase of the gas to liquid velocity ratio $U \geq 2$. Furthermore, because the dominant growth rate and dominant wave numbers are nearly same in both circumstances, the instability zones of both modes stay unchanged. Therefore, we conclude that the gas to liquid velocity ratio $U \geq 2$ has a destabilizing effect on the considered system. It is also clear from Figures 7a,b that increase the gas to liquid velocity ratio in the range $0 < U \leq 1$ decreases the dominant growth rate, and the dominant wave number as well as critical wave number, showing thereby the stability effect of the gas to liquid velocity ratio $U \leq 1$ including the case of zero gas velocity. Figures 7a,b clearly also show that increase the gas to liquid velocity ratio in the range $1 \leq U \leq 2$ leads to increasing the instability zones for both antisymmetric and symmetric modes of disturbances similar to curves in Figures 6a,b. Therefore, we conclude that the gas to liquid velocity ration in range $1 \leq U \leq 2$ has a destabilizing effect. Hence, the gas to liquid velocity ratio has only a stabilizing effect in the range $U \leq 1$, otherwise it has a destabilizing effect on the system. Note that the values of $U = (0.2, 1.8), (0.3, 1.7), ...$etc has the same growth rate curve. In other words, we can conclude that the gas to liquid velocity ratio has a dual role on the stability of the system stabilizing for the ratio range $U \leq 1$, and then destabilizing otherwise for ratio $U \geq 1$.

7.7. Effect of dimension

Figures 8a,b give the relation between the non-dimensional growth rate Ω_r and non-dimensional wave number K for both antisymmetric and symmetric modes, respectively, in two dimensional $N = 0$ and three-dimensional $N \geq 1$ cases of the problem of the stability of an electrified viscoelastic Rivlin-Ericksen liquid sheet streaming with relative velocity in an inviscid gas medium. It is clear from the figures that the growth rates of two-dimensional antisymmetric and symmetric disturbances always exceed that of the three-dimensional ones, and also the three-dimensional disturbance with $N = 1$ has higher growth rates than those with $N = 2$. As a result, we draw the conclusion that, in both cases of antisymmetric and symmetric disturbances, two-dimensional instability disturbances are more unstable than three-dimensional instability ones, and the instability zone in the antisymmetric mode of instability is larger than the corresponding zone in the symmetric mode. As a result, the studied viscoelastic liquid sheet breaks apart more quickly in two dimensions than it does in three. Additionally, this liquid sheet breakdown occurs more quickly in the event of antisymmetric disturbances than it does in the case of symmetric disturbances.

8. Concluding remarks

A linear electrohydrodynamic instability analysis of an incompressible viscoelastic dielectric liquid sheet of Rivlin-Ericksen type streaming with relative velocity in an inviscid dielectric gas medium has been investigated in this paper using the equations of motion for fluids and electric fields with the appropriate boundary conditions. By using the linear temporal stability analysis method, the analytical dimensionless dispersion relations are derived for both an-

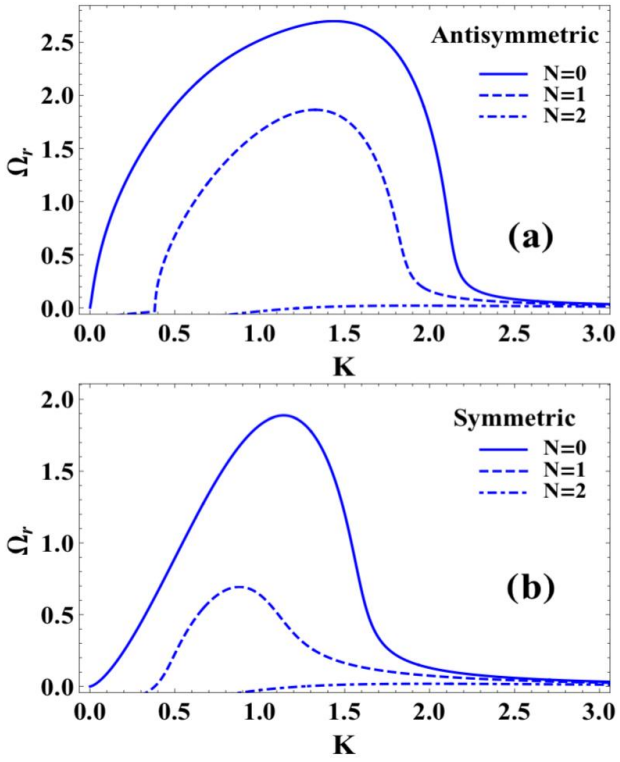

Fig. 8. Variation of growth rate Ω_r with wave number k for various values of two and three dimension N when $We = 10000$, $Oh = 0.1$, $\rho = 0.01$, $V' = 0.01$, $E = 2$, $\tilde{\epsilon_l} = 0.1$, $\tilde{\epsilon_g} = 0.3$ and $U = 1.2$ in (a) antisymmetric and (b) symmetric modes.

tisymmetrical and symmetrical cases. The influence of different elements on the instability of such a liquid sheet problem can be investigated by solving the resulting dispersion relations numerically using the Gaster technique and Mathematica software. Some concluding observations can be made based on the previous analysis and numerical discussion.

- For all the physical parameters included in the analysis, the maximum growth rates and the dominant wave numbers of the antisymmetric mode of disturbance are much greater than in the symmetric mode.
- In both examples of antisymmetric and symmetric modes, the disturbances caused by two-dimensional instability are greater than those caused by three-dimensional instability.
- In both symmetric and antisymmetric modes of disturbance, the electrified viscoelastic liquid sheets can break up more quickly by increasing the electric field, Weber numbers, and gas to liquid density ratio.
- For both kinds of disturbance, increasing the viscoelasticity parameter can reduce the breakup of the electrified viscoelastic liquid sheet.
- The gas to liquid velocity ratio and the Ohnesorge number both affect the system's stability in different ways.

9. Appendix

(1) Numerical Program used to draw Figure 1a, we write

$M = \sqrt{K^2 + n^2}$; $\beta = -K$;

$\Omega = \alpha + i\beta\sqrt{\text{we}}$;

$\Lambda = \Omega + iK\sqrt{\text{we}}$;

we = 10000; $z = 0.1$; $\rho = 0.01$; $n = 0$; $\nu = 0.01$; $B = 0$; $\epsilon 1 = 0.1$;
$\epsilon 2 = 0.3$; $U = 1.2$;

$$F(\mathrm{K\_},\alpha\_) = \left(\Lambda+4M^2(\nu\Omega+z)\right)\Lambda\tanh(M)+4M^3(\nu\Omega+z)^2 \left(M\tanh(M)-\sqrt{M^2+\frac{\Lambda}{\nu\Omega+z}}\tanh\sqrt{M^2+\frac{\Lambda}{\nu\Omega+z}}\right) -\frac{B^2K^2\tanh(M)(\epsilon1-\epsilon2)^2}{\epsilon2\tanh(M)+\epsilon1}+\rho\left(\Omega+iKU\sqrt{\mathrm{we}}\right)^2+M^3$$

$$F_1 = \Re(\mathrm{Table}[\{K,\alpha/.\mathrm{FindRoot}[F(K,\alpha)=0,\{\alpha,5\}]\}, \{K,0.001,5,0.005\}]);$$

$$\mathrm{F11} = \mathrm{ListLinePlot}\left[F_1,\mathrm{PlotStyle}\rightarrow\{\mathrm{Black}\}\right]$$

we obtained the solid curve.

$$\mathrm{we}=10000;\ z=0.1;\ \rho=0.01;\ n=0;\ \nu=0.01;\ B=1;\ \epsilon1=0.1;\ \epsilon2=0.3;\ U=1.2;$$

$$G(\mathrm{K\_},\alpha\_) = \left(\Lambda+4M^2(\nu\Omega+z)\right)\Lambda\tanh(M)+4M^3(\nu\Omega+z)^2 \left(M\tanh(M)-\sqrt{M^2+\frac{\Lambda}{\nu\Omega+z}}\tanh\sqrt{M^2+\frac{\Lambda}{\nu\Omega+z}}\right) -\frac{B^2K^2\tanh(M)(\epsilon1-\epsilon2)^2}{\epsilon2\tanh(M)+\epsilon1}+\rho\left(\Omega+iKU\sqrt{\mathrm{we}}\right)^2+M^3$$

$$G_1 = \Re(\mathrm{Table}[\{K,\alpha/.\mathrm{FindRoot}[G(K,\alpha)=0,\{\alpha,5\}]\}, \{K,0.001,5,0.005\}]);$$

$$\mathrm{G11} = \mathrm{ListLinePlot}\left[G_1,\mathrm{PlotStyle}\rightarrow\{\mathrm{Dashed},\mathrm{Black}\}\right]$$

we obtained the dashed curve.
Show[F11, G11]
we obtained the solid curve and the dashed curve.

$$\mathrm{we}=10000;\ z=0.1;\ \rho=0.01;\ n=0;\ \nu=0.01;\ B=2;\ \epsilon1=0.1;\ \epsilon2=0.3;\ U=1.2;$$

$$H(\mathrm{K\_},\alpha\_) = \left(\Lambda+4M^2(\nu\Omega+z)\right)\Lambda\tanh(M)+4M^3(\nu\Omega+z)^2 \left(M\tanh(M)-\sqrt{M^2+\frac{\Lambda}{\nu\Omega+z}}\tanh\sqrt{M^2+\frac{\Lambda}{\nu\Omega+z}}\right) -\frac{B^2K^2\tanh(M)(\epsilon1-\epsilon2)^2}{\epsilon2\tanh(M)+\epsilon1}+\rho\left(\Omega+iKU\sqrt{\mathrm{we}}\right)^2+M^3$$

$$H_1 = \Re(\mathrm{Table}[\{K,\alpha/.\mathrm{FindRoot}[H(K,\alpha)=0,\{\alpha,5\}]\}, \{K,0.001,5,0.005\}]);$$

$$\mathrm{H11} = \mathrm{ListLinePlot}\left[H_1,\mathrm{PlotStyle}\rightarrow\{\mathrm{DotDashed},\mathrm{Black}\}\right]$$

we obtained the dot dashed curve.

$$\mathrm{Show}\left[\mathrm{F11},\mathrm{G11},\mathrm{H11},\mathrm{PlotRange}\rightarrow\{\{0,3\},\{0.07,2\}\}\right]$$

we obtained solid curve, dashed curve and dot dashed curve.

$$\mathrm{we}=10000;\ z=0.1;\ \rho=0.01;\ n=0;\ \nu=0.01;\ B=3;\ \epsilon1=0.1;\ \epsilon2=0.3;\ U=1.2;$$

$$
\begin{aligned}
J(\mathrm{K\_},\alpha\_) &= \left(\Lambda+4M^2(\nu\Omega+z)\right)\Lambda\tanh(M)+4M^3(\nu\Omega+z)^2 \\
&\left(M\tanh(M)-\sqrt{M^2+\frac{\Lambda}{\nu\Omega+z}}\tanh\sqrt{M^2+\frac{\Lambda}{\nu\Omega+z}}\right) \\
&-\frac{B^2K^2\tanh(M)(\epsilon1-\epsilon2)^2}{\epsilon2\tanh(M)+\epsilon1}+\rho\left(\Omega+iKU\sqrt{\mathrm{we}}\right)^2+M^3
\end{aligned}
$$

$$
\begin{aligned}
J_1 &= \Re(\mathrm{Table}[\{K,\alpha/.\,\mathrm{FindRoot}[J(K,\alpha)=0,\{\alpha,5\}]\}, \\
&\{K,0.001,3,0.01\}]);
\end{aligned}
$$

$\mathrm{J11} = \mathrm{ListLinePlot}\left[J_1, \mathrm{PlotStyle}\rightarrow\{\mathrm{Dotted},\mathrm{Black}\}\right]$

we obtained the dotted curve.

$\mathrm{Show}\left[\mathrm{F11},\mathrm{G11},\mathrm{H11},\mathrm{J11},\mathrm{PlotRange}\rightarrow\{\{0,2.5\},\{0,1.6\}\}\right]$

we obtained the solid curve, the dashed curve, the dot dashed curve and the dotted curve.

M1 = Plot[1.5, {t, 1.8, 2.1}, PlotStyle → {Black}];
M2 = Plot[1.36, {t, 1.8, 2.1}, PlotStyle → {Black, Dashed}];
M3 = Plot[1.2, {t, 1.8, 2.1}, PlotStyle → {Black, DotDashed}];
M4 = Plot[1.05, {t, 1.8, 2.1}, PlotStyle → {Black, Dotted}];
Y1 = Show[F11, G11, H11, J11, M1, M2, M3, M4,
Epilog → {Text[E=0, {2.3, 1.9}, {0, 5}], Text[E=1, {2.3, 1.75}, {0, 5}],
Text[E=2, {2.3, 1.6}, {0, 5}],
Text[E=3, {2.3, 1.45}, {0, 5}], Text[Oh = 0.1, {5.43, 3}, {0, 5}],
Text[ρ = 0.01, {5.56, 2.8}, {0, 5}], Text[We = 1000, {5.5, 2.6}, {0, 5}],
Text[**"Antisymmetric"**, {2.1, 2.1}, {0, 5}], Text["(a)" , {2.2, 1}, {0, 5}],
Frame → True, FrameLabel → {$\mathbf{K}, \Omega_{\mathbf{r}}$},
FrameStyle → $Directive[Black, 16]$,
TextStyle → {FontWeight → "Bold", PlotRange → {{0, 2.5}, {0.1, 1.75}}]

(2) Numerical Program to draw Figure 1b, we will follow the same steps as in the previous case useb in Figure 1a except that any (tanh) will be replaced by (coth), and the last paragraph in this case will be written as

M1 = Plot[0.84, {t, 1.48, 1.72}, PlotStyle → {Black}];
M2 = Plot[0.77, {t, 1, 48, 1.72}, PlotStyle → {Black, Dashed}];
M3 = Plot[0.7, {t, 1.48, 1.72}, PlotStyle → {Black, DotDashed}];
M4 = Plot[0.7, {t, 1.48, 1.72}, PlotStyle → {Black, Dotted}];
Y1 = Show[F11, G11, H11, J11, M1, M2, M3, M4,
Epilog → {Text[E=0, {1.85, 1.04}, {0, 5}], Text[E=1, {1.85, 0.97}, {0, 5}],
Text[E=2, {1.85, 0.9}, {0, 5}],
Text[E=3, {2.3, 1.45}, {0, 5}], Text[Oh = 0.1, {5.43, 3}, {0, 5}],
Text[ρ = 0.01, {5.56, 2.8}, {0, 5}], Text[We = 1000, {5.5, 2.6}, {0, 5}],
Text[**"symmetric"**, {1.75, 1.16}, {0, 5}], Text["(b)" , {1.7, 0.55}, {0, 5}],
Frame → True, FrameLabel → {$\mathbf{K}, \Omega_{\mathbf{r}}$},
FrameStyle → $Directive[Black, 16]$,
TextStyle → {FontWeight → "Bold", PlotRange → {{0, 2.0}, {0.05, 1}}]

Acknowledgments : Our sincere thanks go to the journal's editor and to the anonymous reviewers who contributed detailed comments and suggestions to improve the paper.

References

[1] V.G. Levich, Physcochemical Hydrodynamics; Prentice-Hall, Englewood Cliffs, New Jersy, 1962.
[2] R.B. Bird, R.C. Armstrong, O. Hassager, Dynamics of Polymeric Liquids, vol. 1: Fluid Mechanics, Wiley, New York, 1977.
[3] J.-P. Hsu, A. M. Spasic, Interfacial Electroviscoelasticity and Electrophoresis, CRC Press, Taylor and Francis Group, USA, 2010.
[4] A. H. Lefebvre, Atomization and Spray, Hemisphere, New York, 1989.
[5] K. Masters, Spray Drying Handbook, 4th Ed. John Wiley, New York, 1985.
[6] A. L. Yarin, Free Liquid Jets Films: Hydrodynamics and Rheology; John Wiley & Sons, 1993.
[7] S. P. Lin, Breakup of Liquid Sheets and Jets, 2nd Edition; Cambridge University Press, New York,2010.
[8] X. Li, R. S. Tankin, On the temporal instability of a two-dimensional viscous liquid sheet, Journal of Fluid Mechanics 1991, 226, 425-443.
[9] J. Cousin, C. Dumouchel, Effect of viscosity on the linear instability of a flat liquid sheet, Atomization and Sprays 1966, 6, 563-576.
[10] D. Dasgupta, S. Nath, D. Bhanja , Linear instability analysis of viscous planar liquid sheet sandwiched between two moving gas streams in B. B. Biswal et al.(eds.), Advances in Mechanical Engineering, Lecture Notes in Mechanical Engineering, Springer Nature Singapore Pte Ltd 2021, 41-50.
[11] Y. Han, Kelvin-Helmholtz instability of a confined nano-liquid sheet with the effects heat and mass transfer and marangoni convection, Atomization and Sprays 2022, 32, 73-89.
[12] J. R. Melcher, Continuum Electromechanics, MIT Press, Cambridge, Mass., 1981.
[13] M. F. El-Sayed, Electrohydrodynamic instability of a dielectric fluid layer between two semi-infinite identical conducting fluids in porous medium, Physica A 2006, 367. 25-41,
[14] G. M. Moatimid, Y.O. El-Dib, M. H. Zekry, Instability analysis of a streaming electrified cylindrical through porous media, Pramana 2019, 92, article 22.
[15] D. P. H. Smith, The electrohydrodynamic atomization of liquids, IEEE Transaction on Industry Applications, 1986, IA-22, 527-535.
[16] A. G. Baily, Electrostatic Spraying of Liquids; John Wiley & Sons, New York, 1988.
[17] E. Gileadi, M. (Eds). Urbakh, Thermodynamics and Electrified Interfaces; Willey-VCH Verlag, Weinheim, 2002.
[18] K. Sung, C. S. Lee, Factors influencing liquid breakup in electrohydrodynamic atomization, Journal of Applied Physics, 2004, 96, 3956-3961.
[19] Y.-H. Lee, J. Zhang, D.-R. Chen, Note: Electrohydrodynamic atomization of liquid sheet, Review of Scientific Instruments, 2011, 82, 026111.
[20] G. Brenn, Z. Liu, F. Durst, Three-dimensional temporal instability of non-Newtonian liquid sheet, Atomization and Sprays 2001, 11, 49-84.
[21] L.-J. Yang, Y.-Y. Qu, Q.-F. Fu, B. Gu, F. Wang, Linear stability analysis of a non-Newtonian liquid sheet, Journal of Propulsion and Power 2010, 26, 1212-1224.
[22] L. Yang, Y. Liu, Q. Fu,; C. Wang, Y. Ning, Linear stability analysis of electrified viscoelastic liquid sheets, Atomization and Sprays 2012, 22, 951-982.
[23] M. F. El-Sayed, G. M. Moatimid, F. M. F. Elsabaa, M. F. E. Amer, Hydrodynamic instabilities of two viscoelastic liquid sheet models in an inviscid gas medium, Atomization and Sprays 2015a, 25, 123-151.
[24] M. F. El-Sayed, G. M. Moatimid, F. M. F. Elsabaa, M. F. E. Amer, Electrohydrodynamic instability of non-Newtonian dielectric liquid sheet issued into streaming dielectric gaseous environment, Interfacial Phenomena & Heat Transfer 2015b, 3, 159-183.
[25] M. F. El-Sayed, G. M. Moatimid, F. M. F. Elsabaa, M. F. E. Amer, Electrohydrodynamic instability of non-Newtonian dielectric liquid jet moving in a streaming dielectric gas with a surface tension gradient, Atomization and Sprays 2016, 26, 349-376.
[26] R. S. Rivlin, J. L. Ericksen, Stress-deformation relaxations for isotropic materials, Journal of Rational Mechanics and Analysis 1955, 4, 323-425.
[27] D. D. Joseph, Fluid Dynamics of Viscoelastic Liquids; Springer, New York, 1990.
[28] S. Nath, A. Muklopadhyay, A. Datta, S. Sen,; T. J. Tharakan, Influence of gas velocity on breakup pf planar liquid sheets sandwiched between gas streams, Atomization and Sprays 2010, 20, 983-1003.
[29] S. Nath, A. Muklopadhyay, A. Datta, S. Sarkar, S. Sen, Effect of confinement on breakup of planar liquid sheets sandwiched between two gas streams and resulting spray characteristics, Fluid Dynamic Research 2014, 46, 015511.
[30] S. Chandrasekhar, Hydrodynamic and Hydromagnetic Stability; Dover Publication, New York, 1981.
[31] P. G. Drazin, W. H. Reid, Hydrodynamic Stability; Cambridge University Press, Londen, U. k., 1985.
[32] M. F. El-Sayed, Electro-aerodynamic instability of a thin dielectric liquid sheet sprayed with an air stream, Phys.

Rev, E 1999, 60, 7588-7591.
[33] M. F. El-Sayed, Three-dimensional electrohydrodynamic temporal instability of a moving dielectric liquid sheet emanated into a gas medium, European Physical Journal E 2004, 15, 443-455.
[34] I. Hayati, A. I. Bailey, Th. F. Tadros, Investigations into the mechanisms of electrohydrodynamic spraying of liquids, J. Colloid Interface Sci. 1987, 117, 205-230.
[35] Z. Liu, C. Brenn, F. Durst, Linear analysis of the stability of two-dimensional non-Newtonian liquid sheets, Journal of Non-Newtonian Fluid Mechanics 1998, 78, 133-166.
[36] M. F. El-Sayed, M. H. M. Moussa, A. A. A. Hassan, N. M. Hafez, Electrohydrodynamic instability of liquid sheet saturating porous medium with interfacial surface charges, Atomization and Sprays 2013, 23, 165-191.
[37] E. A. Ibrahim, E. T. Akpan, Three-dimensional instability of viscous liquid sheets, Atomization and Sprays 1996, 6, 649-665.
[38] M. A. Gaster, note on the relation between temporally-increasing and spatially-increasing disturbances in hydrodynamic stability, J, Fluid Mech. 1962, 14, 222-224.
[39] D. E. A. Muller, method for solving algebraic equations using an automatic computer, Mathematical Tables and Aids to Computation 1956, 10, 208-215.
[40] R. Negeed, S. Hidaka, M. Hohno, Y. Takata, Experimental and analytical investigation of liquid sheet breakup characteristics. International Journal of Heat and Fluid Flow 2011, 32, 95-106.
[41] W. Witherspoon, R. N. Parthasarathy, Breakup of viscous liquid sheets subjected to symmetric and asymmetric gas flow, Journal of Energy Resources Technology 1997, 119, 184-192.